World Electric Vehicle Journal

MDPI

Article

Numerical Simulation of Aerodynamic Characteristics of Electric Vehicles with Battery Packs Mounted on Chassis

Yaoji Deng [1,*], Keyu Lu [1], Tao Liu [1], Xufei Wang [2], Hui Shen [1] and Junjie Gong [1]

[1] College of Mechanical Engineering, Yangzhou University, Yangzhou 225127, China; 13584609603@163.com (K.L.); mz120220875@stu.yzu.edu.cn (T.L.); hshen@yzu.edu.cn (H.S.); gjunj@126.com (J.G.)
[2] School of Mechanical Engineering, Shaanxi University of Technology, Hanzhong 723000, China; wxf@snut.edu.cn
* Correspondence: yjdeng@yzu.edu.cn

Abstract: Aerodynamic characteristics are of great significance to the fuel economy and handling the stability of electric vehicles. The battery pack of electric vehicles has a huge structure and is usually arranged in the chassis area of the vehicle, which inevitably occupies the space at the bottom of the vehicle and affects the aerodynamic characteristics of the vehicle. To study the effect of the power battery pack installed in the chassis on the aerodynamics characteristics of the electric vehicle, the Computational Fluid Dynamics (CFD) method is used to study the flow and pressure fields of the SAE (Society of Automotive Engineers) hierarchical car model with battery packs mounted on chassis. The influence of the structure parameters of the battery pack on the automobile's aerodynamics are also analyzed in detail. Based on the simulation results, it can be seen that the battery pack installed on the chassis has a great impact on the flow and pressure field at the bottom and tail of the vehicle, causing the drag coefficient and lift coefficient to increase. The structural parameters of the battery pack have contradictory effects on the drag and lift coefficients. As the length of the battery pack increases, the drag coefficient decreases, and the lift coefficient increases. As the battery pack width and height increase, the drag coefficient increases, and the lift coefficient decreases. The research results provide a reference for the optimization of the aerodynamic characteristics of electric vehicles with battery packs mounted on chassis.

Keywords: aerodynamic characteristic; CFD; battery pack; chassis; electric vehicle

Citation: Deng, Y.; Lu, K.; Liu, T.; Wang, X.; Shen, H.; Gong, J. Numerical Simulation of Aerodynamic Characteristics of Electric Vehicles with Battery Packs Mounted on Chassis. *World Electr. Veh. J.* **2023**, *14*, 216. https://doi.org/10.3390/wevj14080216

Academic Editors: Michael Fowler and Ghanim A. Putrus

Received: 15 July 2023
Revised: 31 July 2023
Accepted: 10 August 2023
Published: 13 August 2023

1. Introduction

Today, energy and environmental issues have become more and more prominent. Compared with traditional fuel vehicles, electric vehicles can effectively reduce their dependence on petroleum resources and alleviate energy and environmental pressure [1,2]. Therefore, electric vehicles can be said to be a more energy-saving and environmentally friendly means of transportation, and it is also considered to be the direction of the future development of the automotive industry [3]. In recent years, the rapid development of electric vehicles has also encountered a "bottleneck". It is difficult to make major breakthroughs in battery technology, and the driving range of electric vehicles is insufficient. Hence, in the current situation, in which battery technology is not high, electric vehicles must improve power efficiency as much as possible. Among them, reducing aerodynamic resistance provides a convenient way for electric vehicles to improve the efficiency of electricity consumption, because aerodynamic resistance accounts for a large part of the vehicle's electrical energy consumption. When the car is running at a high speed, it can account for about 50% of the total consumption [4]. Therefore, it is very meaningful and necessary to conduct aerodynamic research on electric vehicles and improve their aerodynamic characteristics.

The main research methods of automobile aerodynamics can be divided into three types: experimental research, theoretical analysis and numerical calculation. Experimental research includes wind tunnel tests and actual road tests. A wind tunnel test is an important research method of automobile aerodynamics that can be divided into two types: real-vehicle wind tunnel tests and model wind tunnel tests [5,6]. The real-vehicle wind tunnel test can truly simulate the aerodynamic characteristics of the vehicle and obtain more accurate test data. However, this method is very costly and usually only used for real-vehicle verification and the calibration of wind tunnel test results [6–8]. The model wind tunnel test adopts a reduced ratio model for the automobile and is carried out under the condition of meeting similar conditions. This method is convenient to measure and has a low cost. However, the test flow field cannot be completely similar to the flow field of the actual vehicle during operation, and it needs to solve reasonably technical issues, such as the ground effect, the blocking effect and cave wall interference, to obtain accurate wind tunnel test data. The actual road test can test the aerodynamic characteristics of the vehicle in various complex environments and operating conditions. However, the actual road test's cost is relatively high, the test time is longer, and the test results are easily affected and restricted by the driver's subjective factors and objective factors such as road conditions and weather. Therefore, this method is not widely used at present.

The theoretical analysis method is used to establish a mathematical model based on actual problems. In the research of automobile aerodynamics, the theoretical analysis method is used to transform the problem of automobile flow into a mathematical problem and to solve it by using boundary conditions and initial conditions. The theoretical analysis method generally can only model simple problems and cannot satisfy the research and analysis of more complex phenomena.

In recent years, high-performance computers and relatively accurate turbulence models have made calculation fluid dynamics (CFD) methods more and more important in automotive aerodynamics research. Kabanovs investigated the influence of the wheel, ground and spray boundary conditions on a simulation of the rear soiling of a generic SUV using CFD technology [9]. Liu adopted a dynamic mesh and sliding interface to conduct a numerical simulation to investigate the transient aerodynamic characteristics of vehicles during the overtaking process under the influence of crosswinds [10]. Keogh studied the aerodynamic changes that occur during cornering and the underlying physical causes of time-averaged cornering-specific flow phenomena [11]. Cho used the numerical simulation method to evaluate the performance of underbody aerodynamic drag reduction devices based on the actual shape of a sedan-type vehicle [12]. Buljac computationally studied the influence of the rear wing mounting height on automobile aerodynamics by using Reynolds-averaged Navier-Stokes equations, the standard k-ε turbulence model and standard wall functions [13]. Kang developed an actively translating rear diffuser device to reduce the aerodynamic drag experienced by passenger cars, and Computational Fluid Dynamics (CFD) analyses were performed under moving ground and rotating wheel conditions [14]. Kim numerically designed the grille opening shape for small passenger car by using a parametric study [15]. Ljungskog investigated the effects of the inlet yaw angle, inlet pitch angle, basic suction scoop mass flow, first distributed suction mass flow, second distributed suction mass flow and belt speed on the longitudinal pressure distribution in the test section of the Volvo Cars aerodynamic wind tunnel using CFD [16]. Beigmoradi optimized of rear end of a simplified car model considering aerodynamic and acoustic objectives [17].

Many researchers have conducted a lot of research on the aerodynamic characteristics of traditional fuel vehicles with numerical calculation methods, and they have achieved fruitful results [18–24]. However, the development trend of integration and the application of electronic and electrical technology make electric vehicles different from traditional fuel vehicles in terms of the structural layout. The biggest difference is that the battery replaces the fuel tank and becomes the power source of the vehicle. Because the battery pack layout needs to consider many factors, such as the layout space, collision safety, heat dissipation,

etc., how to arrange the battery pack reasonably has become a new problem. Due to the large size and limited layout space, the chassis is the most popular placement location of battery packs, and the battery pack often protrudes from the chassis. This phenomenon is very common in small electric vehicles. This arrangement compresses the space between the chassis and the road, changes the shape of the bottom of the car and has a certain impact on the airflow at the bottom of the car. Currently, the structural difference between this electric vehicle and the traditional fuel vehicle has not attracted enough attention, and related research on aerodynamics has not yet started.

This article focuses on the effect of a battery pack mounted on the chassis on the outflow and pressure field of electric vehicles in steady-state motion and conducts a parametric analysis to study the influence of the structural parameters of the battery pack on the aerodynamic characteristics of the vehicle. The research results provide a reference for the arrangement of battery packs mounted on the chassis from an aerodynamics point of view and have great significance for perfecting the aerodynamic performance of electric vehicles and improving vehicle fuel economy and handling stability. This paper is structured as follows: The CFD methodology is outlined in Section 2, the numerical simulation calculation process is introduced in Section 3, the results for the aerodynamics simulations and discussion are presented in Section 4, and the conclusions are presented in Section 5.

2. Fundamental Theory of Computational Fluid Dynamics

Computational Fluid Dynamics (CFD) is the analysis of systems that include intersecting physical phenomena, such as fluid flow and heat conduction, through computer numerical calculations and image displays [25]. At present, continuously developing numerical simulations based on CFD have become an important research method in automobile aerodynamics. It can essentially be regarded as a numerical simulation of fluid flow under the control of basic flow equations. Through a numerical simulation, the basic physical quantities (such as the distribution of pressure, velocity, temperature, etc.) at various points in the flow field of a very complex problem can be obtained, as well as the instantaneous changes in these physical quantities.

2.1. Governing Equations of Fluid Dynamics

Fluid flow must comply with the laws of conservation of physics, which mainly include the law of conservation of mass, the law of conservation of momentum and the law of conservation of energy.

Any fluid flow problem must follow the law of conservation of mass. This law can be described as follows. The increase in the mass of a fluid micro-element in a unit of time is equal to the net mass flowing into the micro-element in the same time period.

$$\frac{\partial \rho}{\partial t} + \frac{\partial(\rho u)}{\partial x} + \frac{\partial(\rho v)}{\partial y} + \frac{\partial(\rho w)}{\partial z} + 0 \tag{1}$$

where ρ is the density of the fluid; t is the time; and u, v and w are the components of the velocity vector u of the fluid in the x, y and z directions, respectively. For an incompressible fluid, P is a constant, so Equation (1) becomes Equation (2).

$$\frac{\partial \rho}{\partial t} + div(\rho u) = 0 \tag{2}$$

The momentum conservation equation is also necessary for any fluid flow system. The law can be expressed as follows. The rate of change in the momentum of a fluid in a micro-element body with respect to time is equal to the sum of various forces acting on the micro-element body from the outside.

$$\frac{\partial(\rho u)}{\partial t} + div(\rho u U) = div(\mu grad u) - \frac{\partial p}{\partial x} + S_u \tag{3}$$

$$\frac{\partial(\rho v)}{\partial t} + div(\rho vU) = div(\mu gradv) - \frac{\partial p}{\partial y} + S_v \tag{4}$$

$$\frac{\partial(\rho w)}{\partial t} + div(\rho wU) = div(\mu gradw) - \frac{\partial p}{\partial z} + S_w \tag{5}$$

Equations (3)–(5) are the momentum conservation equations of the three components in the x, y and z directions, referred to as the momentum conservation equation, also known as the Navier-Stokes equation; S_u, S_v and S_w are the generalized source terms of the momentum conservation equation; P is the pressure on the fluid element; and u is the dynamic viscosity of the fluid.

The energy conservation equation is a basic law that must be satisfied by a flow system that includes heat exchange. The law can be expressed as follows. The rate of the increase in energy in a micro-element body is equal to the net heat flow into the micro-element body plus the work performed by the physical and surface forces on the micro-element body.

The relationship between internal energy i and temperature T is $I = C_P T$, where C_P is the specific heat capacity. In this way, the energy conservation equation (6) with temperature T as the variable can be obtained.

$$\frac{\partial(\rho T)}{\partial t} + div(\rho UT) = div\left(\frac{k}{c_p} gradT\right) + S_T \tag{6}$$

where C_P is the specific heat capacity; T is the temperature; k is the heat transfer coefficient of the fluid; and S_T is the internal heat source of the fluid and the part where the mechanical energy is converted into heat energy, also called the viscous dissipation term.

For incompressible fluids, if the amount of heat exchange is small or even negligible, it is possible to solve the continuum equation and the momentum equation simultaneously without considering the energy conservation equation.

2.2. Numerical Discretization Method

Before performing CFD calculations, it is necessary to discretize the computational domain. According to the different principles of discretization, three methods are roughly formed, namely the Finite Difference Method (FDM), the Finite Element Method (FEM) and the Finite Volume Method (FVM). The FDM is the earliest and most classic numerical solution method, and it is an approximate numerical solution method that directly transforms a differential problem into an algebraic problem. The FEM is a widely used fluid dynamics numerical calculation method that absorbs the core of discrete processing in the FDM and uses the selection approximation function in the variational calculation to integrate the area. It is a new numerical discrete method formed by the combination of numerical methods and analytical methods. The FEM has a strong solving ability, can adapt to very complicated geometry, can deal with various types of boundary conditions uniformly and is conducive to the preparation of general calculation programs.

The FVM is a discretization method that has developed rapidly in recent years. It is characterized by high computational efficiency and flexible meshing and can approximate complex geometric models. At present, the FVM has been widely used in the field of CFD, and its characteristics are well reflected in both the discrete results of the governing equations and the grid used. At present, most Computational Fluid Dynamics software used in the automotive industry uses the FVM, such as STAR-CD, CFX, FLUENT, etc.

2.3. Turbulence Simulation Method

Turbulent flow is a common, highly nonlinear and complex flow phenomenon in nature. Therefore, it is currently difficult to use analytical methods to study turbulent flow phenomena. However, it can be simulated with some numerical simulation methods. With the development of computer technology, results that are more consistent with reality

have been obtained, and the accuracy of numerical simulations can also meet the needs of general engineering.

Turbulence simulation methods are divided into direct simulations and indirect simulations. Direct simulations directly solve the instantaneous turbulence control equation. Their biggest advantage is that they do not need to make any simplifications to the flow, and they theoretically obtain more accurate results. Indirect simulations approximate and simplify the turbulent flow using certain rules instead of directly calculating the turbulence characteristics. Although direct simulations are better than indirect simulations in terms of accuracy, direct numerical simulation methods have higher requirements on computers. Current computer technology cannot meet their requirements, so they cannot be applied to actual engineering calculations. Therefore, indirect numerical simulation methods are generally used in actual engineering calculations.

This paper uses the turbulence model in the Reynolds averaging method. The core idea is to skip solving the instantaneous Navier-Stokes equation and find a way to solve the time-averaged Reynolds equation. The purpose of this is to avoid a large number of calculations, and good results have been achieved in actual engineering calculations.

3. Numerical Simulation Calculation

3.1. Geometric Model of SAE Model

In this paper, the standard SAE step back car model is selected as the prototype [26]. The structure of the model is relatively simple, the body has no complex accessories, and the chassis of the model is simplified as a smooth plate. The three-dimensional geometric model is established in CATIA V5R21 software, as shown in Figure 1.

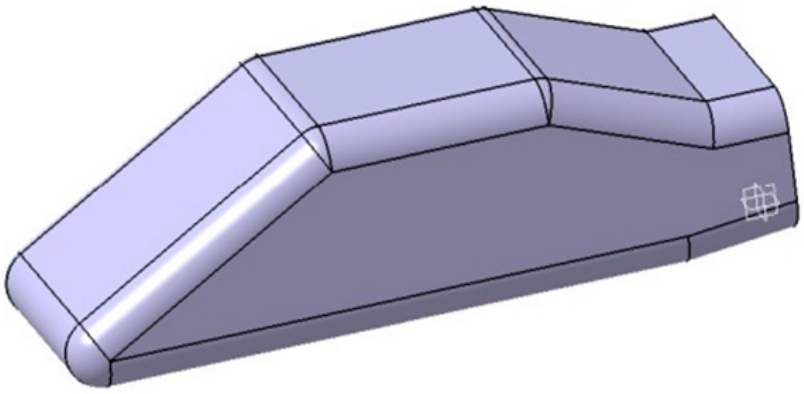

Figure 1. SAE notchback car model.

Considering that most of the battery pack structure is cuboid, the part of the battery pack protruding from the bottom of the car is simplified as a cuboid, and the length, width and height of the battery pack are 300 mm, 200 mm and 274 mm, respectively. Because the main research content of this paper is the influence of the structural parameter of the battery pack on the aerodynamic performance, the length A, width B and height H of the battery pack are selected as the changing parameters. L is the distance between the front end of the battery pack and the front of the vehicle. The range of the change of the selected parameters takes into account ergonomics and, at the same time, meets the basic crash requirements and trafficability of the electric automobile. The structure of the electric automobile model with a battery pack is shown in Figure 2.

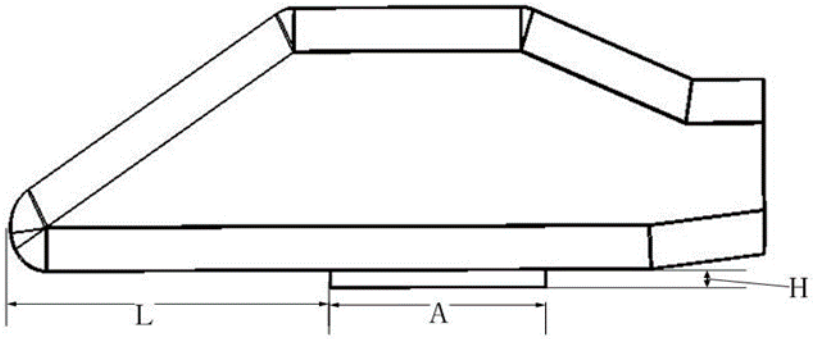

(**a**)

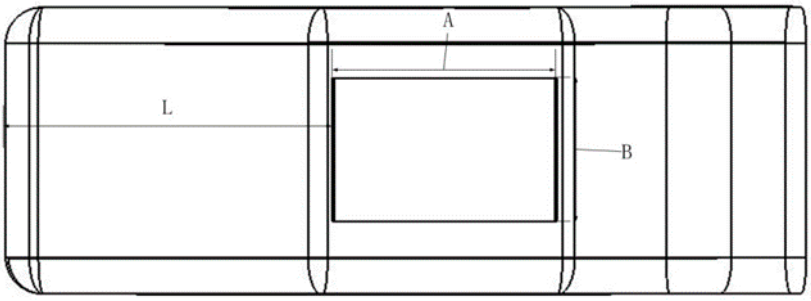

(**b**)

Figure 2. Schematic arrangement of battery pack: (**a**) Front view; (**b**) Top view.

3.2. Computational Domain

The basic principles for determining the size of the calculation domain are as follows: (1) The influence on the flow field around the car is not significant, and the characteristics of the flow field around the car body can be captured as much as possible. (2) The size of the calculation domain should not be too large, which is conducive to reducing the number of calculations, shortening the cycle and improving the efficiency [26].

From the actual situation, the scope of the calculation domain should be set to infinity, but with the increase in the scope of the calculation domain, the calculation time also increases greatly, which completely depends on the system configuration of the running simulation. However, the effect of air far away from the car body is very small and can be ignored. Therefore, in the actual numerical simulation, it is set in a limited area. In general, the scope of the calculation domain is defined on the basis of the model size. The size of the calculation domain selected in this paper meets the following requirements: the space in front of the car is taken as three times the car length, the space above the roof is taken as five times the car height, the space on the side of the car is taken as five times the car width, and the space behind the car is taken as five times the car length. In this way, the whole computational domain is a cuboid with a length of 37,800 mm, a width of 11,200 mm and a height of 7200 mm.

3.3. Grid Generation

In the numerical calculation, grid generation is of great significance, and the quality, form and density of the grid have an important impact on the accuracy and efficiency of the CFD calculation. ICEM-CFD, as a popular pre-processing software, can provide a high-quality grid for mainstream CFD 15.0 software and meet the strict requirements of grid generation.

The three-dimensional model established in CATIA is exported to STP format and imported into ICEM-CFD 15.0 software for meshing. The strategy of a tetrahedral and triangular prism hybrid grid is adopted, and the octree algorithm is used to generate the tetrahedral grid. The maximum size of the global grid is 600 mm. The density box is

used to encrypt the local area around the car body, and the encryption size is 60 mm. In order to better simulate the boundary layer effect, the aerodynamic coefficient is accurately captured, and the requirements of the wall function are met. Six layers of the triangular prism mesh with a growth ratio of 1.2 are stretched out on the body surface, and the total thickness is 8 mm. Finally, the generated mesh is smoothed, and the mesh quality in the final calculation domain is greater than 0.3, as shown in Figure 3.

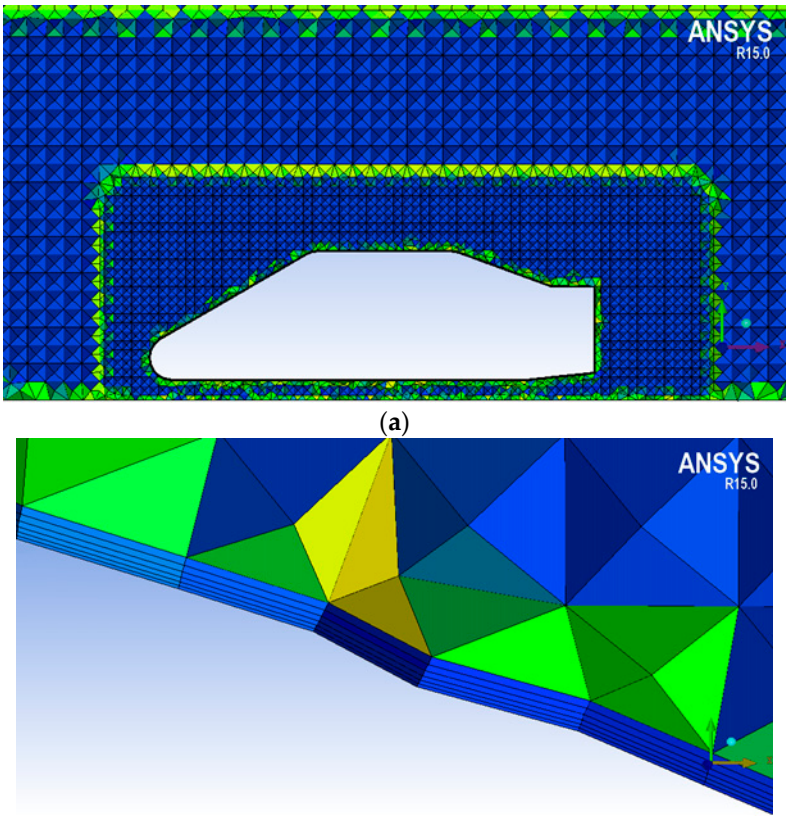

Figure 3. Grid distribution: (**a**) Grid distribution of longitudinal symmetry planes; (**b**) Boundary layer mesh.

3.4. Turbulence Model and Wall Function

In this paper, the simulated vehicle speed is far lower than the sound speed, so the flow field around the vehicle can be regarded as a three-dimensional incompressible viscous isothermal flow field. Compared with the standard $k-\varepsilon$ model, the $RNG\ k-\varepsilon$ turbulence model takes the turbulence vortex into account, which has higher reliability and accuracy and needs less calculation time and memory, so it is suitable for the calculation of complex flow fields outside the automobile.

In the fluid boundary layer region, the turbulence effect is very obvious, and a high-Reynolds-number model is not suitable in this region. However, sometimes, in order to reduce the number of grids near the surface of the object, a high-Reynolds-number model must be used. In this case, the wall function is needed to calculate the turbulent physical quantities at the wall. In this paper, a combination of the non-equilibrium wall functions and the $RNG\ k-\varepsilon$ turbulence model is used to simulate.

3.5. Boundary Conditions

Setting the boundary conditions correctly is critical for the FLUENT 15.0 software to calculate accurate results. The inlet boundary of the calculation area is set as the velocity boundary condition, and the inlet velocity and other related parameters are required. The boundary condition at the outlet is set as the pressure outlet condition, and the static

pressure of the outlet is required. The left and right surfaces and the upper surface of the calculation area adopt a slip wall boundary. In order to truly simulate the relative movement between the ground and the car, the ground is set as a moving wall boundary, and the moving speed needs to be given. The body surface adopts a non-slip wall boundary. The specific boundary condition parameter settings are shown in Table 1.

Table 1. Boundary condition parameters settings.

Boundary	Type	Numerical Value
Inlet	Velocity-inlet	V = 20–40 m/s, Direction is perpendicular to the inlet; turbulence intensity I = 0.5%
Left, right and top surfaces	Sliding wall boundary	
Body surface	No sliding wall boundary	
Ground	Moving wall boundary	V = 20–40 m/s, Direction is opposite to the wind speed
Outlet	Pressure outlet	Standard atmospheric pressure

4. Simulation Results and Discussion

In the Fluent 15.0 software, the solver selects the pressure-based coupling solver, the pressure–velocity coupling mode selects the SIMPLE algorithm, and the gradient discrete format selection is based on the Least Squares Cell-Based method. The maximum residual error is set to 0.0005. After many attempts, the pressure, momentum and density sub-relaxation factors are set to 0.7, 0.7 and 1 respectively. The monitoring curve of the aerodynamic coefficients is also set. When each scheme is calculated to approximately 1800 steps, the variable residual curve and the aerodynamic coefficient curve tend to be stable, which can be considered as convergence.

4.1. Grid Number Independence Analysis and Model Verification

The grid is the geometric expression of the CFD model, and the density of the grid has a great influence on the results of the numerical simulation. Only when the increase in the grid number has a small influence on the results, the numerical simulation results are meaningful. The same grid strategy is adopted for the calculation model, and the influence of different grid numbers on the calculation results is analyzed. Table 2 shows the calculation process and the results of different grid numbers. After the grid number iteration test, about 9.3 million grids can guarantee the accuracy of the calculation and need less calculation time.

Table 2. Grid independence test.

Mesh Quantity/Million	Drag Coefficient	Lift Coefficient	Convergence Time/h
2.5	0.2011	−0.2011	4
4.7	0.1978	−0.2076	7
9.3	0.1931	−0.2139	16
14.1	0.1931	−0.2140	24

Figure 4 shows the distribution of the y^+ values on the surface of the car. It can be seen from the figure that the y^+ values are mainly concentrated from 30 to 160, which satisfies the application of the unbalanced wall function and turbulence model and also verifies the rationality of meshing.

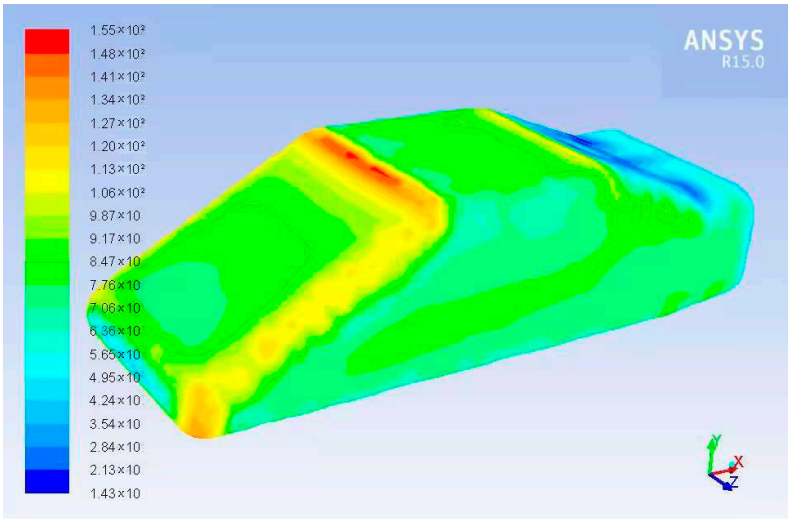

Figure 4. Distribution of y^+ body surface.

4.2. Aerodynamic Analysis of Electric Vehicle with Battery Packs Mounted on Chassis

4.2.1. Aerodynamic Coefficient Analysis

Numerical simulations are performed on the aerodynamic characteristics of the original model and the model with the battery pack, and the drag coefficient and lift coefficient are obtained, as shown in Table 3. From Table 3, it can be seen that the drag coefficient and lift coefficient of the model with the battery pack increase compared with those of the original model. The battery pack has an adverse effect on the drag coefficient and lift coefficient, and the effect of the battery pack on the drag coefficient is greater than that on the lift coefficient, which seriously affects the fuel economy of the electric vehicle.

Table 3. Comparison of drag and lift coefficient of two models.

Wind Speed / Model	20 m/s		40 m/s	
	Drag Coefficient	**Lift Coefficient**	**Drag Coefficient**	**Lift Coefficient**
Original model	0.1913	−0.2453	0.1931	−0.2439
Model with battery pack	0.2296	−0.2398	0.2274	−0.2374
Variation	20.0%	2.2%	17.8%	2.7%

4.2.2. Outflow and Pressure Field Analysis

Because the battery pack is arranged at the classis of the electric vehicle, we focus on comparing the outflow and pressure fields on the bottom and the rear of vehicle between the original model and the model with a battery pack.

Figure 5 shows the bottom streamline diagram of the original model and the model with a battery pack. It can be seen from the figure that the bottom streamline of the original model is very smooth, the airflow flows through very smoothly, and the pressure is small, resulting in a relatively small friction loss of the airflow through the bottom of the vehicle body, thereby reducing aerodynamic drag. With the addition of the battery pack, the airflow becomes complicated due to the obstruction of the battery pack. Part of the airflow flows to both sides of the battery pack, obvious airflow separation occurs when flowing through the corners of the battery pack, and the other airflow flows to the bottom of the battery pack. Two parts of the airflow converge at the rear end of the battery pack to form two obvious vortices. The energy in the vortex dissipates, and a negative pressure zone is formed. Moreover, the battery pack increases the windward area of the lower surface of the car and increases the aerodynamic drag coefficient of the car.

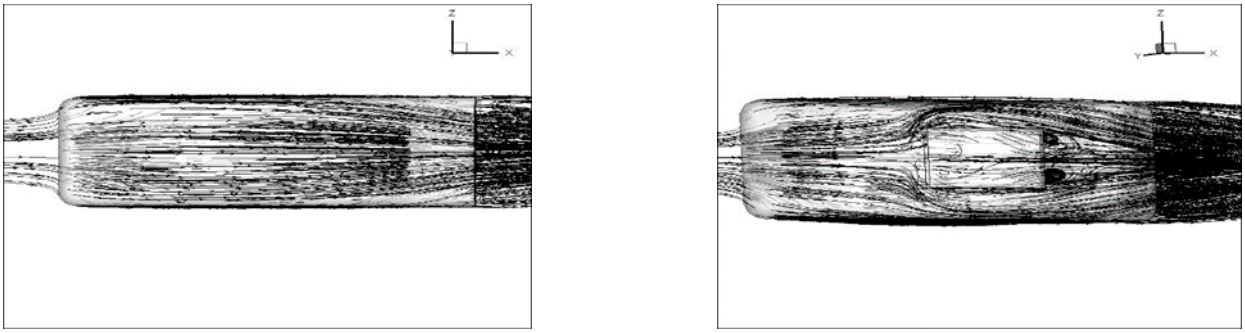

(**a**) (**b**)

Figure 5. Underbody streamlines of original model and model with battery pack: (**a**) Original model; (**b**) Model with battery pack.

Figure 6 presents the bottom pressure distribution of the original model and the model with a battery pack. The battery pack compresses the originally narrow bottom space, and the airflow into the bottom of the battery pack accelerates. However, compared with the smooth bottom of the original model, the airflow is obstructed by the battery pack, and the overall airflow velocity at the bottom is reduced. According to Bernoulli's principle, the flow rate of the airflow at the bottom decreases, and the upward pressure at the bottom rises, resulting in increased aerodynamic lift.

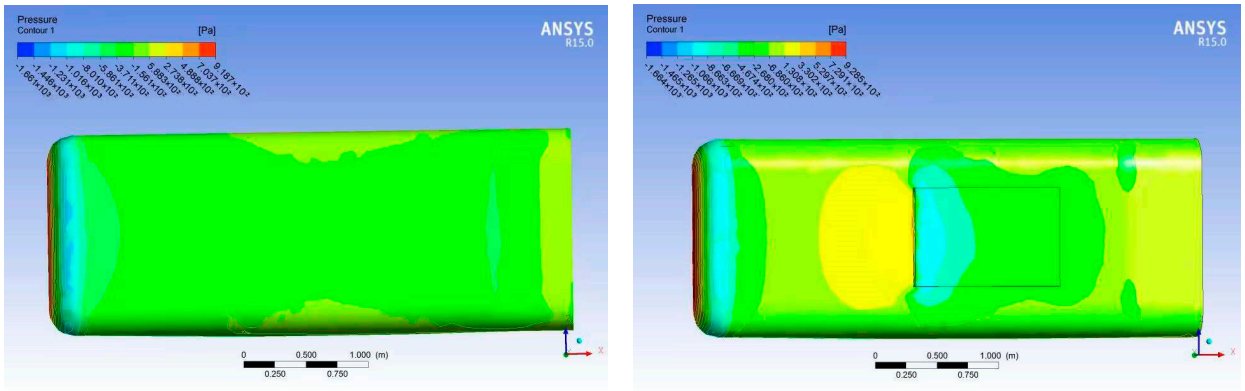

(**a**) (**b**)

Figure 6. Underbody pressure distribution of original model and model with battery pack: (**a**) Original model; (**b**) Model with battery pack.

Figure 7 shows the longitudinal velocity vector diagram of the tail airflow of the original model and the model with a battery pack. Comparing Figure 7a,b, it can be found that the effect of the battery pack on the airflow field at the rear of the car is very significant. The wake vortex of the original model is not very obvious, and the phenomenon of reverse flow appears at a distance from the rear of the car. After installing the battery pack, the wake vortex becomes more complicated, and the position of the airflow's backflow advances. This is because the airflow from the rear of the battery pack to the rear of the car is similar to the phenomenon of a sudden change tube. When the air flows through the rear of the battery pack, the flow section suddenly expands, and the airflow separation phenomenon occurs when the airflow approaches and leaves the corner. This results in energy loss, reduces the average airflow velocity and eventually slows down the airflow velocity reaching the rear of the car, weakening the upward curling tendency. It cannot smoothly merge with the airflow from the upper surface of the car at the rear of the car, which makes the vortex intensity at the rear of the car stronger. The pressure at the rear of the car decreases, and the differential pressure resistance increases.

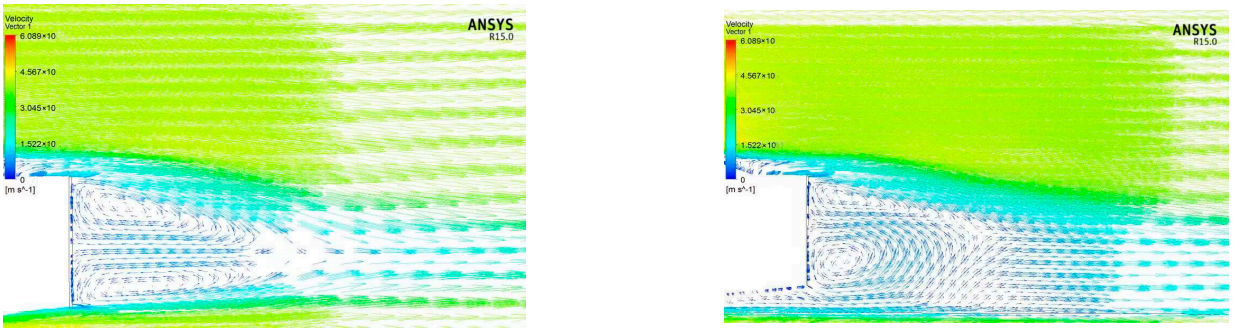

(**a**) (**b**)

Figure 7. Velocity vector comparison of longitudinal symmetric plane in tail region: (**a**) Original model; (**b**) Model with battery pack.

Figure 8 shows the turbulent kinetic energy of the original model and the model with a battery pack in the tail region. It can be seen that, after the battery pack is installed, the airflow at the rear of the car is turbulent, and the turbulence intensity significantly increases, especially the turbulence intensity in the center area of the vortex in the wake. The high turbulence intensity means that the turbulence dissipation rate is also large. Thus, energy consumption is also increased, resulting in an increase in aerodynamic resistance.

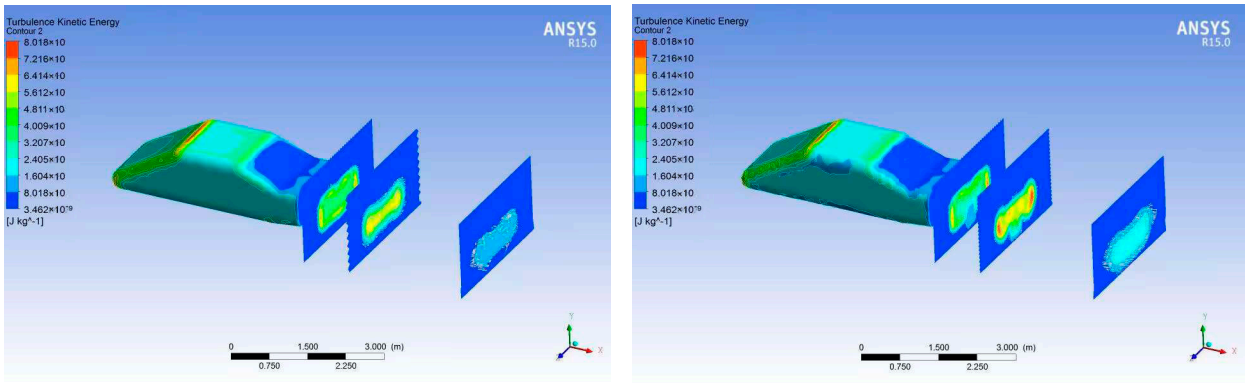

(**a**) (**b**)

Figure 8. Turbulence kinetic energy of the original model and the model with a battery pack in the tail region: (**a**) Original model; (**b**) Model with battery pack.

4.3. Effect of the Structural Parameters of the Battery Pack on the Aerodynamic Coefficient

Through the numerical simulation of the aerodynamic characteristics of the vehicle model with different structure parameters of the battery pack, the relationship between the structure parameters and the aerodynamic coefficient of the battery pack is found, which lays the foundation for the optimization of the structure of the battery pack and the improvement of the aerodynamic performance of electric vehicles. In order to study the influence of the structure parameters of the battery pack on the aerodynamic performance of the electric vehicle, by changing the research parameters of the battery pack and keeping the other parameters of the battery pack unchanged, the corresponding simulation model is established for numerical simulations, and the influence of the rules of the research parameters of the battery pack on the drag coefficient and lift coefficient are obtained.

Figure 9 shows the effect of the battery length on the aerodynamic drag coefficient and lift coefficient. It can be seen that, as the length of the battery pack increases, the drag coefficient decreases, and the lift coefficient increases. This is because, as the battery becomes longer, the airflow becomes more obviously affected by the attached surface layer, the airflow velocity to the rear of the battery pack becomes slower, the vortex strength becomes weaker, the positive pressure at the front of the battery pack remains unchanged,

the differential pressure resistance decreases, and the resistance coefficient decreases. The increase in the length of the battery pack results in the thickening of the surface layer, which compresses the airflow channels, reduces the airflow velocity, increases the pressure and increases the lift coefficient.

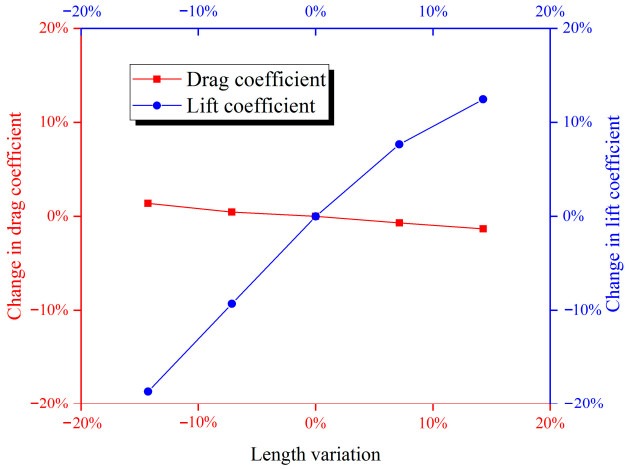

Figure 9. Drag and lift coefficients varying with the length of the battery pack.

Figure 10 shows the effect of the battery width on the aerodynamic drag coefficient and lift coefficient. It can be seen from the simulation results that, with the increase in the battery width, the drag coefficient increases, and the lift coefficient decreases. This is because the increase in the battery width hinders more airflow, the positive pressure zone formed at the front end becomes larger, and the wake vortex at the rear end becomes more complex, resulting in an increase in differential pressure resistance. In addition, as the width of the battery pack increases, the windward area at the bottom of the car increases, resulting in an increase in the drag coefficient. With the increase in battery width, although the positive pressure area at the bottom of the car in front of the battery pack becomes larger, more airflow accelerates when passing under the battery pack. In addition, the negative pressure area at the front and around the battery pack increases, the overall pressure at the bottom of the car decreases, and the lift coefficient decreases.

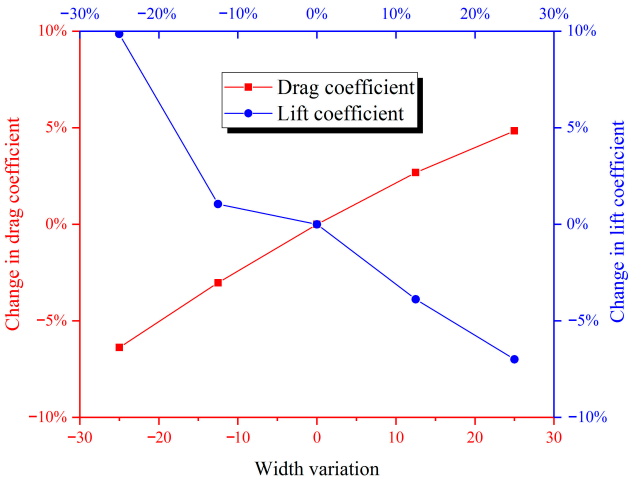

Figure 10. Drag and lift coefficients varying with the width of the battery pack.

Figure 11 shows the effect of the battery height on the aerodynamic drag coefficient and lift coefficient. The simulation results show that, with the increase in the height of the battery, the resistance coefficient increases, and the lift coefficient decreases. This is because the height of the battery increases, which hinders more airflow, and the positive pressure

area at the front end of the battery pack becomes larger. In addition, as the windward area at the bottom of the car becomes larger, the drag coefficient becomes higher. As the height of the battery pack increases, the airflow channel at the bottom of the car becomes smaller, the flow velocity becomes faster, the pressure at the bottom of the car decreases, and the lift coefficient decreases. The increase in the battery height means reducing the minimum ground clearance of vehicles. The research of the SAE model in the literature [25] shows that, when the minimum ground clearance of the vehicle is more than 100 mm, the lift coefficient increases with the increase in the ground clearance, which is consistent with the trend of our research.

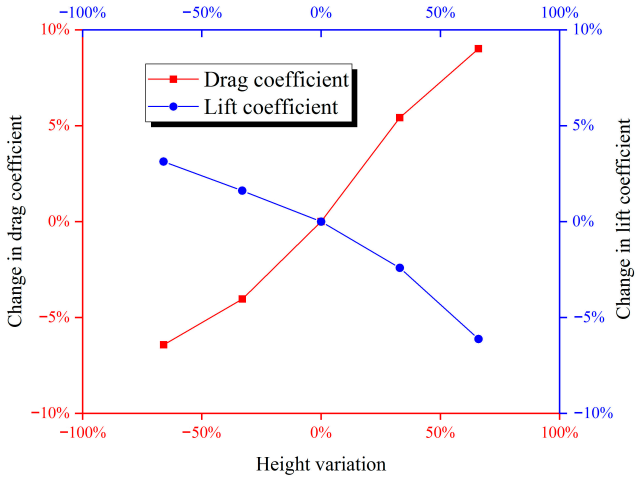

Figure 11. Drag and lift coefficients varying with the height of the battery pack.

5. Conclusions

In this paper, taking an SAE standard vehicle as a prototype, the CFD numerical simulation method is used to study the influence of a bottom battery pack on the aerodynamic characteristics of a vehicle, and the influence of the structure parameters of the battery pack on the aerodynamic coefficient of the vehicle is also analyzed.

On the basis of reasonable simulation settings, the aerodynamic characteristics of the electric vehicle before and after the installation of the battery pack are numerically simulated, and the influence of the battery pack on the aerodynamic characteristics of the vehicle is analyzed. The results show that the bottom battery pack has a negative impact on the aerodynamic characteristics of electric vehicles. In the bottom area of the car, the battery pack blocks the airflow, reduces the airflow velocity and complicates the flow. Two obvious vortices are formed at the rear end of the battery pack. The energy in the vortex area dissipates, forming a negative pressure area, resulting in an increase in aerodynamic resistance and aerodynamic lift. In the rear area of the car, the battery pack makes the wake vortex more complex, the turbulence degree is significantly enhanced, and the position of the airflow's backflow advances.

The aerodynamic characteristics of the vehicle model with different structure parameters of the battery pack are analyzed, and the relationship between the structure parameters of the battery pack and the aerodynamic coefficient of the vehicle is obtained. With the increase in the width of the battery pack, the aerodynamic resistance coefficient increases, whereas the aerodynamic lift coefficient decreases. With the increase in the battery length, the aerodynamic drag coefficient decreases, and the aerodynamic lift coefficient increases. With the increase in the battery height, the aerodynamic drag coefficient increases, and the aerodynamic lift coefficient decreases. It is worth noting that the trend of the influence of the structure parameters of the battery pack on the aerodynamic drag coefficient and aerodynamic lift coefficient is always opposite. Therefore, when designing the structure of the battery pack, we should consider the influence of the resistance coefficient and

lift coefficient at the same time and adjust their weights according to the performance requirements.

Author Contributions: Conceptualization, Y.D. and H.S.; methodology, T.L.; software, Y.D.; validation, X.W.; formal analysis, H.S.; investigation, H.S.; resources, Y.D.; data curation, K.L.; writing—original draft preparation, Y.D.; writing—review and editing, K.L.; visualization, T.L.; supervision, J.G.; project administration, Y.D.; funding acquisition, Y.D. All authors have read and agreed to the published version of the manuscript.

Funding: This work was supported by the Postgraduate Research & Practice Innovation Program of Jiangsu Province [grant number SJCX23_1903] and the Yangzhou City, Yangzhou University co construction of innovation and technology platform project [grant number YZ2020266].

Data Availability Statement: The data that support the findings of this study are available from the corresponding author upon reasonable request.

Acknowledgments: The authors give sincere thanks to the editors and reviewers for their patient work and constructive suggestions.

Conflicts of Interest: The authors declare no conflict of interest.

References

1. Pourasad, Y.; Ghanati, A.; Khosravi, M. Optimal design of aerodynamic force supplementary devices for the improvement of fuel consumption and emissions. *Energy Environ.* **2017**, *28*, 263–282. [CrossRef]
2. Lucas, A.; Silva, C.A.; Neto, R.C. Life cycle analysis of energy supply infrastructure for conventional and electric vehicles. *Energy Policy* **2012**, *41*, 537–547. [CrossRef]
3. Van Vliet, O.; Brouwer, A.S.; Kuramochi, T.; van den Broek, M.; Faaij, A. Energy use, cost and CO_2 emissions of electric cars. *J. Power Sources* **2011**, *196*, 2298–2310. [CrossRef]
4. Hucho, W.H. *Aerodynamics of Road Vehicles*, 4th ed.; SAE International: Warrendale, PA, USA, 1998.
5. Cheli, F.; Corradi, R.; Sabbioni, E.; Tomasini, G. Wind tunnel tests on heavy road vehicles: Cross wind induced loads-Part 1. *J. Wind. Eng. Ind. Aerodyn.* **2011**, *99*, 1000–1010. [CrossRef]
6. Huang, T.; Zhuang, X.; Wan, Z.; Gu, Z. Experimental and numerical investigations of the vehicle aerodynamic drag with single-channel rear diffuser. *Proc. Inst. Mech. Eng. Part D J. Automob. Eng.* **2020**, *234*, 2216–2227.
7. Altinisik, A.; Yemenici, O.; Umur, H. Aerodynamic analysis of a passenger car at yaw angle and two-vehicle platoon. *J. Fluids Eng.* **2015**, *137*, 121107-1–121107-10. [CrossRef]
8. Wieser, D.; Schmidt, H.-J.; Müller, S.; Strangfeld, C.; Nayeri, C.; Paschereit, C. Experimental comparison of the aerodynamic behavior of fastback and notchback driv aer Models. *SAE Int. J. Passeng. Cars-Mech. Syst.* **2014**, *7*, 682–691. [CrossRef]
9. Kabanovs, A.; Garmory, A.; Passmore, M.; Gaylard, A. Investigation into the dynamics of wheel spray released from a rotating tyre of a simplified vehicle model. *J. Wind. Eng. Ind. Aerodyn.* **2019**, *184*, 228–246. [CrossRef]
10. Liu, L.; Sun, Y.; Chi, X.; Du, G.; Wang, M. Transient aerodynamic characteristics of vans overtaking in crosswinds. *J. Wind. Eng. Ind. Aerodyn.* **2017**, *170*, 46–55. [CrossRef]
11. Keogh, J.; Barber, T.; Diasinos, S. The aerodynamic effects on a cornering ahmed body. *J. Wind. Eng. Ind. Aerodyn.* **2016**, *154*, 34–46. [CrossRef]
12. Cho, J.; Kim, T.; Kim, K. Comparative Investigation on the aerodynamic effects of combined use of underbody drag reduvtion devices applied to real sedan. *Int. J. Automot. Technol.* **2017**, *18*, 959–971. [CrossRef]
13. Buljac, A.; Džijan, I.; Korade, I.; Krizmanić, S.; Kozmar, H. Automobile aerodynamics influenced by airfoil-shaped rear wing. *Int. J. Automot. Technol.* **2016**, *17*, 377–385. [CrossRef]
14. Kang, S.O.; Jun, S.O.; Park, H.I.; Song, K.S.; Kee, J.D.; Kim, K.H.; Lee, D.H. Actively translating a rear diffuser device for the aerodynamic drag reduction of a passenger car. *Int. J. Automot. Technol.* **2012**, *13*, 583–592. [CrossRef]
15. Kim, J.M.; Kim, K.M.; Ha, S.J.; Kim, M.S. Grille design for passenger car to improve aerodynamic and cooling performance using CFD technique. *Int. J. Automot. Technol.* **2016**, *17*, 967–976. [CrossRef]
16. Ljungskog, E.; Sebben, S.; Broniewicz, A. A parametric study on the influence of boundary conditions on the longitudinal pressure gradient in CFD simulations of an automotive wind tunnel. *J. Mech. Sci. Technol.* **2017**, *31*, 2821–2827. [CrossRef]
17. Beigmoradi, S.; Hajabdollahi, H.; Ramezani, A. Multi-objective aero acoustic optimization of rear end in a simplified car model by using hybrid robust parameter design, artificial neural networks and genetic algorithm methods. *Comput. Fluids* **2014**, *90*, 123–132. [CrossRef]
18. Wu, H.; Zeng, X.H.; Gao, D.G.; Lai, J. Dynamic stability of an electromagnetic suspension maglev vehicle under steady aerodynamic load. *Appl. Math. Model.* **2021**, *97*, 483–500. [CrossRef]
19. Hua, C.; Zhang, Y.; Dong, D.; Yan, B.; Ouyang, H. Aerodynamic noise numerical simulation and noise reduction study on automobile alternator. *J. Mech. Sci. Technol.* **2017**, *31*, 2047–2055. [CrossRef]

20. Shankar, G.; Devaradjane, G.; Sunil, S. Investigation on aerodynamic behaviour of a SUV car model with vortex generators at different yaw conditions. *J. Appl. Fluid Mech.* **2019**, *12*, 103–117. [CrossRef]
21. Grm, A.; Batista, M. Vehicle aerodynamic stability analysis under high crosswind. *Stroj. Vestn.* **2017**, *3*, 191–200. [CrossRef]
22. Sosnowski, M. The influence of computational domain discretization on CFD results concerning aerodynamics of a vehicle. *J. Appl. Math. Comput. Mech.* **2018**, *17*, 79–88. [CrossRef]
23. Kelly, D.; Batty, J.; Carrel-Billiard, T.; Cybulsky, A.; Viala, L.; Dumas, Y.; Visconti, N.; Mountassir, M.H. Computational-based aerodynamic design for a formula SAE vehicle. *SAE Int. J. Passeng. Cars Mech. Syst.* **2018**, *11*, 35–44. [CrossRef]
24. Huang, T.M.; Gu, Z.Q.; Feng, C.J. Coupled analysis of unsteady aerodynamics and vehicle motion of a passenger car in crosswind condition. *J. Appl. Fluid Mech.* **2017**, *10*, 625–637. [CrossRef]
25. Cogotti, A. *A Parametric Study on the Ground Effect of a Simplified Car Model*; SAE980031; SAE: Warrendale, PA, USA, 1998.
26. Deng, Y.J.; Wang, X.F. Study of aerodynamic characteristics of electric vehicles with battery pack. *J. Shaanxi Univ. Technol.* **2016**, *32*, 15–18.